Journal of Applied Geophysics 112 (2015) 175–189

Contents lists available at ScienceDirect

Journal of Applied Geophysics

journal homepage: www.elsevier.com/locate/jappgeo

Application of EM38 and ERT methods in estimation of saturated hydraulic conductivity in unsaturated soil

Mohammad Farzamian [a,*], Fernando A. Monteiro Santos [a], Mohamed A. Khalil [a,b]

[a] IDL-Universidade de Lisboa, Faculdade de Ciências, Campo Grande, Ed. C8, 1749–016 Lisboa, Portugal
[b] National Research Institute of Astronomy and Geophysics, Helwan, Cairo, Egypt

ARTICLE INFO

Article history:
Received 27 May 2014
Accepted 21 November 2014
Available online 29 November 2014

Keywords:
ERT
EM38
Unsaturated flow simulation
Hydraulic conductivity estimation

ABSTRACT

Soil apparent electrical conductivity is being considerably used as a surrogate measure for soil properties and hydraulic parameters. In this study, measurements of electrical conductivity were accomplished with electrical resistivity tomography (ERT) and EM38 to develop multiple datasets for defining spatiotemporal moisture content variations and estimating saturated hydraulic conductivity under natural conditions in an experimental site located in Lisbon, Portugal. In addition, EM38 capability in monitoring electrical conductivity variations in comparison with ERT method was examined. In order to achieve these objectives, appropriate relationships were derived based on determination of experimental curve resistivity vs. degree of saturation by in-situ investigation to convert electrical resistivity maps inferred from ERT and EM38 data to moisture content distribution maps. In addition, the surface temperature variations during the experiment were measured and the effects of the temperature variations were removed by assuming 2% change in electrical resistivity per °C change in temperature. The conducted experiment proves that the soil is fairly homogenous and semi-pervious sediment and the spatiotemporal moisture content variations during the experiment barely exceed 10%. Our calculations constrain the range of saturated hydraulic conductivity to be 3–9 (cm/day) range.

1. Introduction

The importance of soil characterization in the top 1–2 m is widely recognized as a key parameter in agriculture and is critical for optimal crop management. Development of the means to monitor soil moisture spatiotemporally in agricultural fields is very important for effective soil moisture management. Moreover, hydraulic conductivity is an important soil property when determining the potential for water movement in topsoil and in spite of its importance; soil hydraulic conductivity remains one of the most difficult of soil properties to assess and laboratory methods have limitations due to the size of the samples and usually in-situ methods are required to estimate hydraulic conductivity.

Methods of soil moisture determination are often classified into direct and indirect methods (Muñoz-Carpena, 2004). Direct methods involve taking the weight of a soil sample before and after oven drying. Direct methods are based on drilling and cause major disturbance to the natural conditions. In addition, direct measurements by sample collection cannot be repeated over time on the same place, while hydrologic characterization of topsoil requires a repetition of data collection from a specified field site. Moreover, direct measurements do not usually cover a large area allowing only localized investigation and cause uncertainty in hydrologic characterization of unsaturated zone. Due to the destructive nature of soil sampling, indirect measurements of soil moisture using neutron probes, capacitance probes and time-domain reflectometry are preferred for repeated in-situ measurement of soil moisture. These soil moisture sensors have been extensively used in soil water monitoring under a wide range of soil types, vegetation and experimental sites (e.g. Fares and Alva, 2000; Fares et al., 2004). Evett et al. (2002) presented a comparison of the above mentioned sensors in soil water content measurements under a wide range of soil types on four continents to examine the accuracy and precision of each method and also conditions of successful use. While these in-situ techniques can provide accurate information on soil moisture, the spatial range of the sensors is limited to tens of centimeters and extension of the information to a large area can be problematic.

Recent research has shown that geophysical methods particularly ground-penetrating radar (GPR), ERT and Electromagnetic induction methods (EMI) using non-invasive methods are a viable alternative to traditional techniques for soil characterization. Geophysical methods have been widely used to investigate unsaturated zone (e.g. Binley and Kemna, 2005; Binley et al., 2001, 2002a,b; Huisman et al., 2001, 2002; Looms et al., 2008a,b; Triantafilis and Monteiro Santos, 2010; Triantafilis et al., 2009). Soil apparent electrical conductivity (ECa) is a surrogate measure for soil properties and can be correlated with soil properties such as cation exchange capacity (Triantafilis et al., 2009), depth to bedrock and soil texture (Zhu et al., 2010) or clay content and salinity (Corwin and Lesch, 2005). In addition, time-lapse geophysical monitoring is also a powerful tool to estimate those hydrologic

* Corresponding author. Tel no.: +351217500880.
E-mail address: mohammadfarzamian@fc.ul.pt (M. Farzamian).

http://dx.doi.org/10.1016/j.jappgeo.2014.11.016
0926-9851/

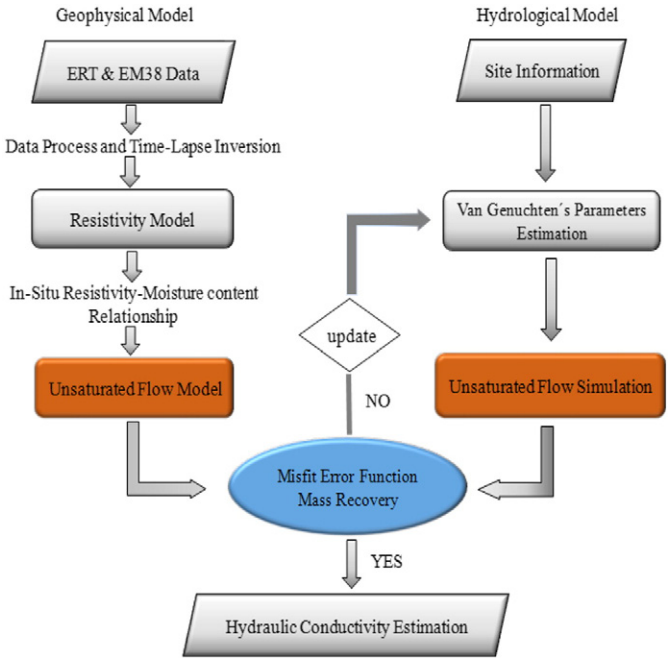

Fig. 1. Analysis flowcharts for integration of geophysical and hydrological data to estimate the saturated hydraulic conductivity.

variables that are time dependent such as water content. The major aim of time-lapse monitoring is to identify changes in resistivity at selected locations at different times accurately. A correlation of hydrological variables to measured responses by empirical or semiempirical relationships (e.g., Archie, 1942) or established in-situ relationships leads mapping hydrogeology variables over time (e.g. Kemna et al., 2002; Singha and Gorelick, 2006).

The main aim of this study is monitoring ECa variations using ground surface ERT and multi-height EM38 methods under natural condition in order to estimate saturated hydraulic conductivity. Several studies (e.g. Binley et al., 2002a; Cassiani et al., 2006; Deiana et al., 2007; Looms et al., 2008a,b) have been conducted to use ERT and GPR methods to estimate hydraulic conductivity; however, to the best of our knowledge, no attempt has been made to use multi-height EM38 data for hydraulic conductivity estimation. EM38 has the advantage of being less expensive, much faster, and easier to use in data collection in comparison with the ERT method. Furthermore, EM38 can cover a larger area in regional investigation. This study also aims to evaluate the EM38 capability in monitoring ECa variations and hydraulic conductivity estimation in comparison with the more commonly used ERT method.

To achieve these objectives, we have followed three steps outlined in Fig. 1.

1. Time-lapse multi-height EM38 and ERT data were inverted to estimate the spatiotemporal resistivity variations.
2. In-situ petrophysical relationship was used to convert the resistivity models to the unsaturated flow models.
3. The unsaturated flow models were compared to the unsaturated flow simulations inferred from hydrologic parameters in order to estimate the saturated hydraulic conductivity.

2. Material and methods

2.1. Study area

The study area is located at the campus of University of Lisbon with a loam soil, low permeability and high water retention capacity. The study was carried out from September 2010 to August 2011. The surface temperature was measured during the experiment. A tipping bucket rain gauge (Young Model 52202) was installed to measure the amount of precipitation during the period of the experiment. Evaporation data was collected from a nearby station to take into account for moisture content simulation. Transpiration was negligible in the field site and was not considered in this study. The mean maximum and minimum temperatures during the experiment period are shown in Fig. 2. In winter, the temperature occasionally dropped as low as 5 °C. The coldest month was January with monthly mean maximum and minimum temperatures of 14 °C and 9 °C. In summer, the temperature never exceeded 36 °C. The hottest month was August with monthly mean maximum and minimum temperatures of 28 °C and 18 °C. The monthly total rainfall and evaporation during the experiment are shown in Fig. 3. December had the highest monthly total rainfall with 294.5 mm and an average of 17 rainy days. June and July were almost without rainfall. The maximum total evaporation was observed in June with a total amounting to 101.9 mm. December had the lowest total evaporation.

2.2. Experimental transect

A profile with 14.25 m length was established to conduct the experiment, on a 2 m unsaturated soil. Four soil cores down to a depth of

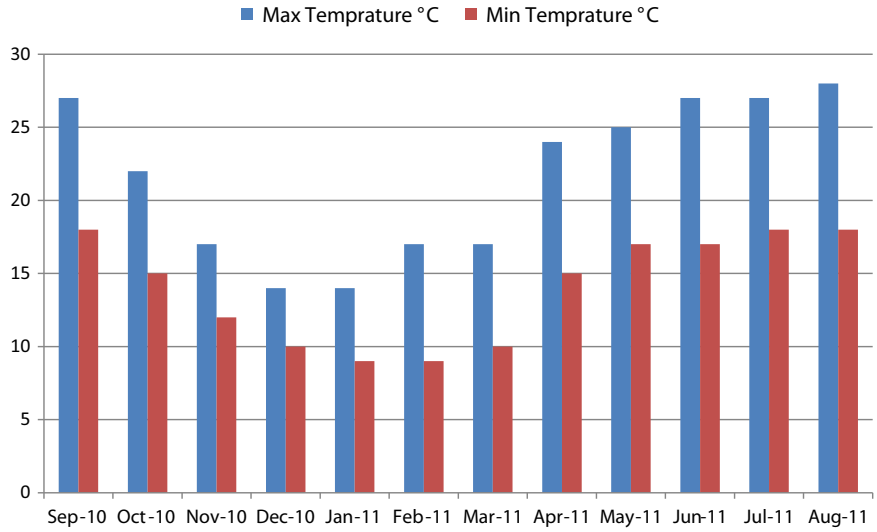

Fig. 2. Monthly means maximum and minimum temperatures (°C) during the study period.

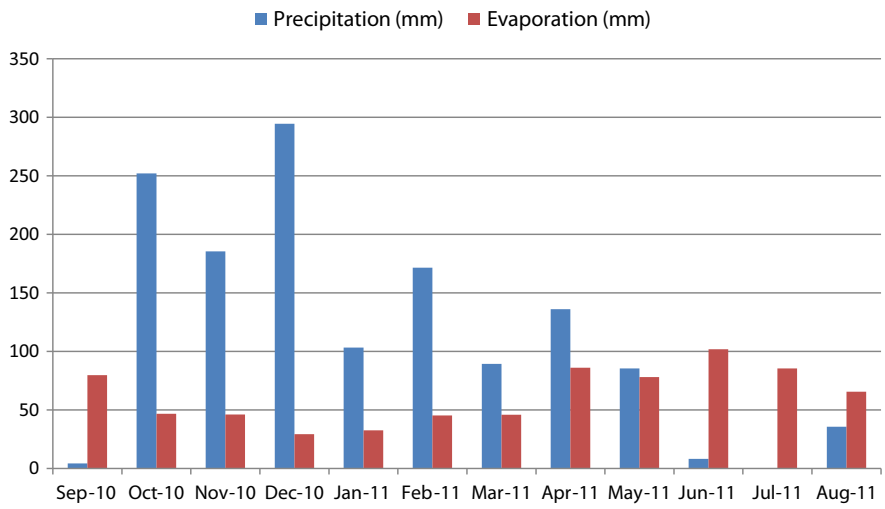

Fig. 3. Monthly total rainfall and evaporation (mm) during the study period.

approximately 1.5–2 m were extracted along the profile in 6 and 9 m in 2-Dec 2010, 3 m in 21-Apr 2011 and 12 m in 20-June 2011. These cores were sectioned into 0.1 m lengths and prepared for laboratory analysis of physical properties namely particle density, bulk density, texture and gravimetric moisture content. Standard set of sieves were used to divide sand into classes, and to separate sand fractions from silt and clay fractions in the soil. To determine the clay to silt ratio, the fraction of the soil passing through the last sieve (0.063 mm) was analyzed using laser granulometer Malvern Particle Size Analyzer MS2000 after deflocculating with 30% sodium hexametaphosphate.

2.3. ERT

ERT is the method for determination of subsurface resistivity distribution from multiple electrical resistance measurements made using a quadrapole arrangement of electrodes. The electrodes are placed either on the ground or in borehole and a 2-D or 3-D image of the resistivity can be achieved by varying the location and spacing of the electrode quadrapole. In this study, a 2-D ground surface ERT survey was performed using 4POINTLIGHT_10W devise from Lippman Company. Geotest software was used for remote controlling of 4POINTLIGHT_10W in combination with active boxes for geoelectric tomography using multi-electrodes. Schlumberger electrode configuration was employed in this study. The maximum current electrode expansion and electrode separation were 14.25 and 0.75 m respectively and a total of 81 measurements were collected for each dataset.

The inversion of time-lapse resistivity data was carried out using RES2DINV software. Several time-lapse inversion algorithms such as, the difference inversion method (LaBrecque and Yang, 2001), the crossmodel regularization (e.g. Loke, 1999; Oldenborger et al., 2007) and 4-D space–time inversion method proposed by Kim et al. (2009) are supported by RES2DINV. Hayley et al. (2011) presented a comprehensive explanation and comparison of the above mentioned methods and showed that the 4-D space–time inversion method reduces the inversion artifacts and better reproduces the resistivity model among the time-lapse inversion methods. This method introduces the regularizations not only in the space domain but also in time to reduce inversion artifacts and improve stability of the inverse problem even if changes in the subsurface properties during the data acquisition cannot be ignored. The 4-D space–time inversion method was used in this study.

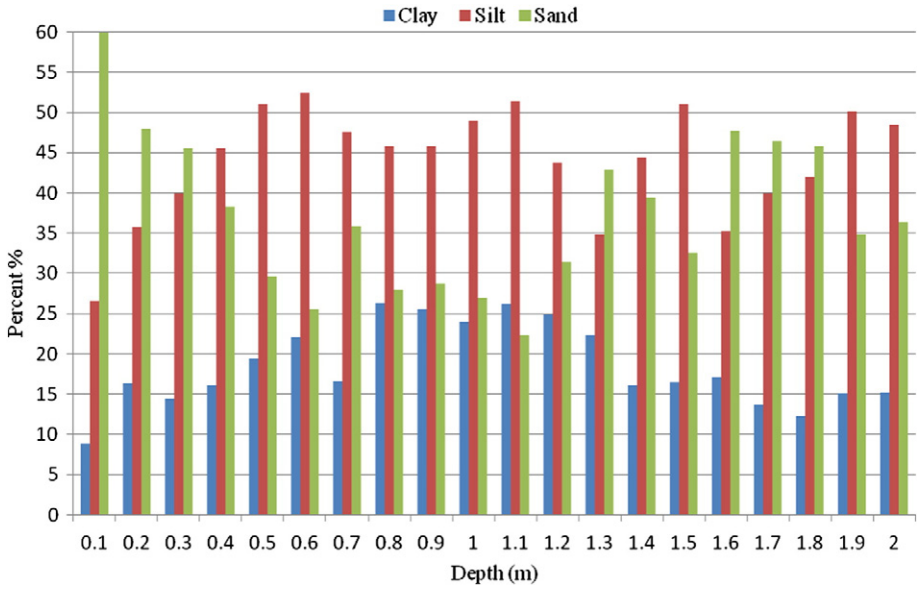

Fig. 4. Soil texture grade of extracted soil samples from x = 6 m.

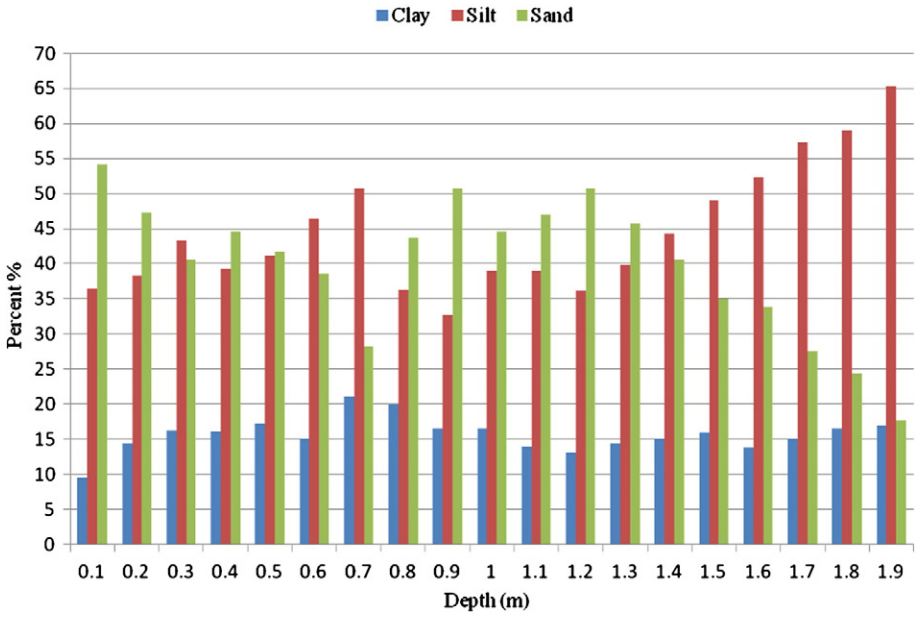

Fig. 5. Soil texture grade of extracted soil samples from x = 9 m.

2.4. The EM38

The EMI technique was initially introduced for measuring and mapping soil salinity (Halvorson and Rhoades, 1974; McNeill, 1986; Wollenhaupt et al., 1986) and was extended to quantifying and mapping soil moisture content. The relationship between soil moisture content and electrical conductivity has been established by many investigators (e.g. Brevik et al., 2006; Hanson and Kaita, 1997; Hezarjaribi and Sourell, 2007; Reedy and Scanlon, 2003; Sheets and Hendrickx, 1995).

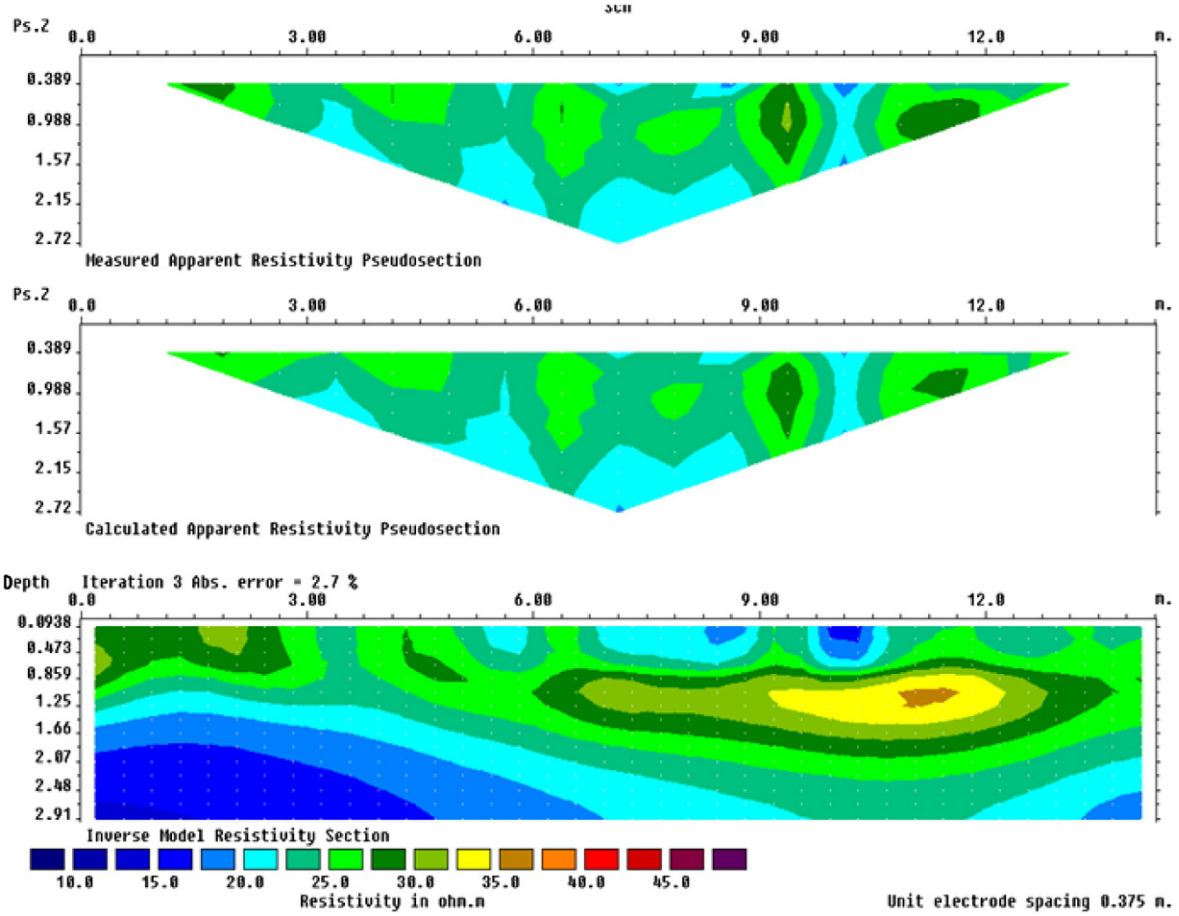

Fig. 6. 2-D resistivity models of ERT background using Schlumberger electrode configuration.

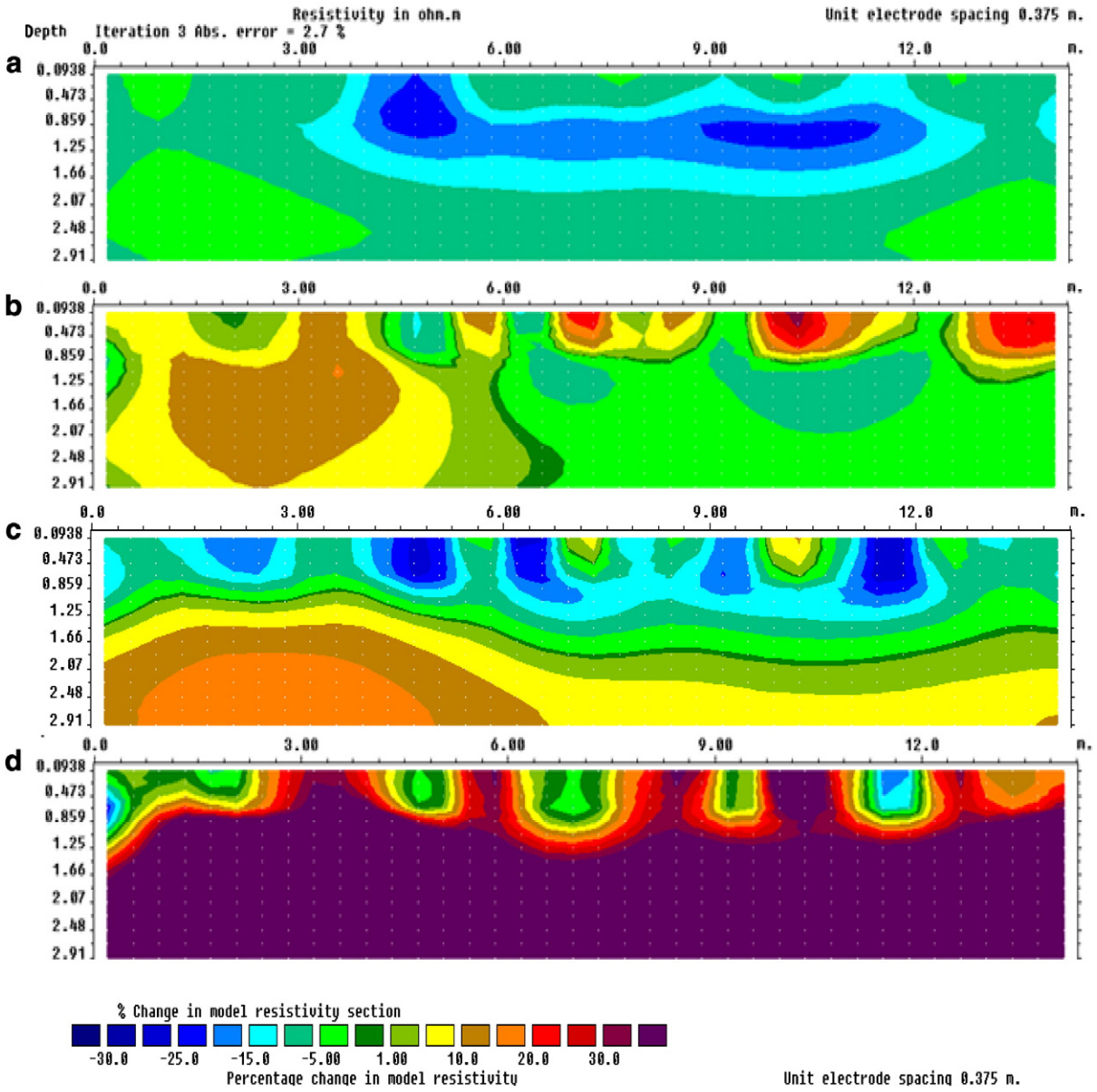

Fig. 7. Sequence of percentage resistivity changes inferred from ERT inversion results with respect to background in a) 4-Nov 2010, b) 11-Feb, c) 21-Apr and d) 20-Jun 2011 respectively.

The EM38 is a widely-used electromagnetic instrument for soil characterization developed by Geonics Ltd. (Ontario, Canada). It comprises two electrical coils, one a transmitter and the other a receiver placed 1 m apart in a wooden frame. The transmitter coil is excited with a sinusoidal current at a frequency of 14.6 kHz. A key assumption in understanding the nature of the integrated response of the surface measurement of the EM38 is that individual; below ground current loops are not influenced by others nearby (McNeill, 1980). Consequently, the net secondary magnetic field at the receiver is the sum of the independent secondary magnetic fields from each of the individual current loops. Then the relative contribution to the secondary magnetic field from all material below a depth z can be expressed by the cumulative function $R_{H,V}$ (for horizontal or vertical coplanar transmitter–receiver dipole configurations) as defined by McNeill (1980):

$$R_{H,V}\int_{z}^{\infty}\varphi_{H,V}(z)dz \tag{1}$$

In this study, EM38 measurements were made in the vertical (EM38v) and horizontal (EM38h) modes of operation with 0.75 m separation along the profile. To facilitate multi-height EM38 measurement, a specially-designed polymer-plastic ladder was constructed at heights corresponding to 0.3, 0.6 and 0.9 m. EM38 measurements were collected in both vertical and horizontal in the mentioned heights. A total of 160 points were measured in each survey.

To invert EM38 data, EM4Soil software has been used. This program was developed using 1-D laterally constrained inversion method proposed by Monteiro Santos (2004). The software was successfully used in several studies (e.g. Triantafilis and Monteiro Santos, 2013; Triantafilis et al., 2012, 2013). The earth model used in the inversion process consists of a number of blocks whose distribution and size depend on the locations and number of intercoil spacing used in data acquisition. A forward modeling subroutine, based on the cumulative response was used to calculate the apparent conductivity response of the model. An iterative process then allows obtaining the final model through the calculated misfit between data and model response given by

$$Q=\left(\frac{\delta d^{T}\delta d}{N}\right)^{1/2} \tag{2}$$

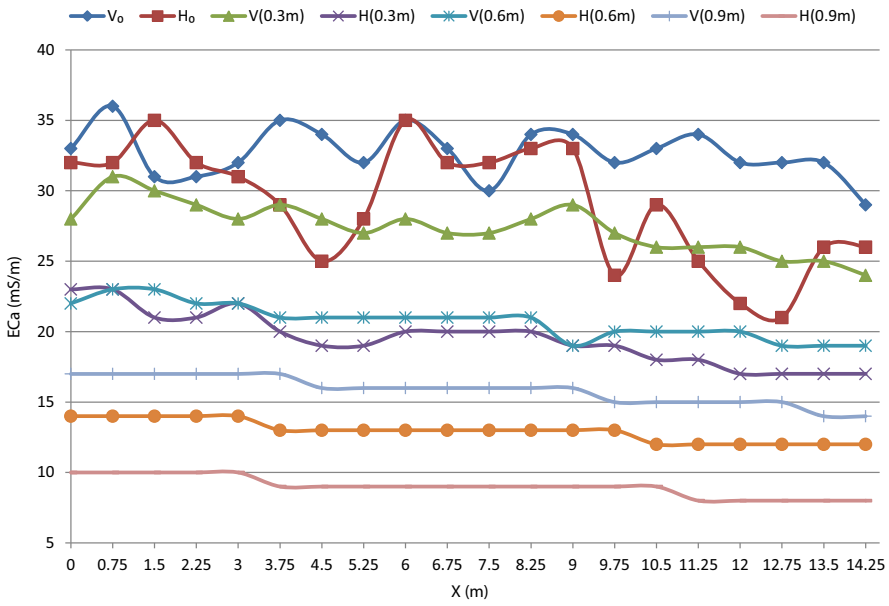

Fig. 8. Spatial distribution of ECa (mS/m) along the profile in 28-Oct 2010 obtained using EM38 in the vertical and horizontal modes of operation on the ground and heights of 0.3, 0.6 and 0.9 m.

where N represents the number of data points (for description of 1-D laterally constrained inversion of EMI data, see, Monteiro Santos, 2004). Independent inversions were carried out for each EM38 dataset separately. Afterward, resistivity changes with time were achieved by subtraction of pixel-by-pixel values from the background image.

2.5. Temperature changes

The goal of this experiment is to monitor electrical resistivity changes due to changes in the moisture content in the unsaturated zone. In order to accomplish this, all other transient factors such as temperature that affect the unsaturated zone must be accounted for. Several attempts have clearly accounted for subsurface temperature variation in resistivity map (e.g. Hauck, 2002; Hayley et al., 2007, 2009; Michot et al., 2003). It is common practice in electrical geophysics to assume a linear variation in resistivity with temperature over the typical range of temperatures encountered in shallow surveys (Musgrave and Binley, 2011). Schön (2004) for instance proposed a 2.5% change in electrical resistivity per °C change in temperature. Hayley et al. (2007), using a variety of near surface materials found out that the slope of the low temperature linear model is quite consistent and a value between 1.8% and 2.2% change in electrical resistivity per °C change in temperature can be used if no other information is available. The effect of temperature variations was removed from the resistivity models by applying a value of 2% change per degree after inversion.

2.6. Hydrologic model

2.6.1. Governing flow equation

Richards' equation is used to describe unsaturated flow in porous media. Two-dimensional Richards' equation can be expressed as (Šimůnek et al., 2006):

$$\partial/\partial x\left[K_H(h)\frac{\partial h}{\partial x}\right]+\partial/\partial z\left[K_V(h)\frac{\partial(h+z)}{\partial z}\right]=\frac{\partial\theta}{\partial t} \tag{3}$$

where h [L] is pressure head, z [L] is elevation, θ is volumetric moisture, $K_H(h)$ and $K_V(h)$ are the horizontal and vertical unsaturated hydraulic conductivity [L/T] respectively as a function of pressure head. The system is isotropic if $K_H(h) = K_V(h)$. Eq. (3) must be supplemented with relevant constitutive models linking h, θ and K.

2.6.2. The unsaturated soil hydraulic properties

The unsaturated soil hydraulic properties, $\theta(h)$ and $K(h)$, in Eq. (3) are in general highly nonlinear functions of the pressure head. We assume here that the retention and hydraulic conductivity functions can be represented by the parametric models of Van Genuchten (1980) who used the statistical pore-size distribution model of Mualem (1976) to obtain a predictive equation for the unsaturated hydraulic conductivity function in terms of soil water retention parameters:

$$\theta(h)=\begin{cases}\theta_r+\dfrac{(\theta_s-\theta_r)}{[1+|\alpha h|^n]^m} & h<0\\ \theta_s & h\geq 0\end{cases} \tag{4}$$

$$K(h)=K_sS_e^l\left[1-\left(1-S_e^{1/m}\right)^m\right]^2 \tag{5}$$

$$S_e=\frac{\theta-\theta_r}{\theta_s-\theta_r} \tag{6}$$

$$m=1-1/n\ ,\ n>1 \tag{7}$$

where θ_s is the saturated moisture content, θ_r is the residual moisture content, defined as the water content for which the gradient $d\theta/dh$ becomes zero, α and n are empirical parameters and K_s is the saturated hydraulic conductivity. The pore connectivity parameter l in the hydraulic conductivity function was estimated (Mualem, 1976) to be about 0.5 as an average for many soils (Šimůnek et al., 2006). To achieve an infiltration model, five van Genuchten's parameters (θ_r, θ_s, α, n, and K_s) must be first estimated. To estimate van Genuchten's parameters, the Rosetta software (Schaap et al., 2001) was used. Rosetta implements pedotransfer functions based on artificial neural networks which predict water retention and saturated hydraulic conductivity from soil textural data and bulk density.

2.6.3. HYDRUS 2D

HYDRUS 2D software package (Šimůnek et al., 2006) was used in this study in order to simulate unsaturated flow. The HYDRUS program numerically solves the Richards equation for unsaturated

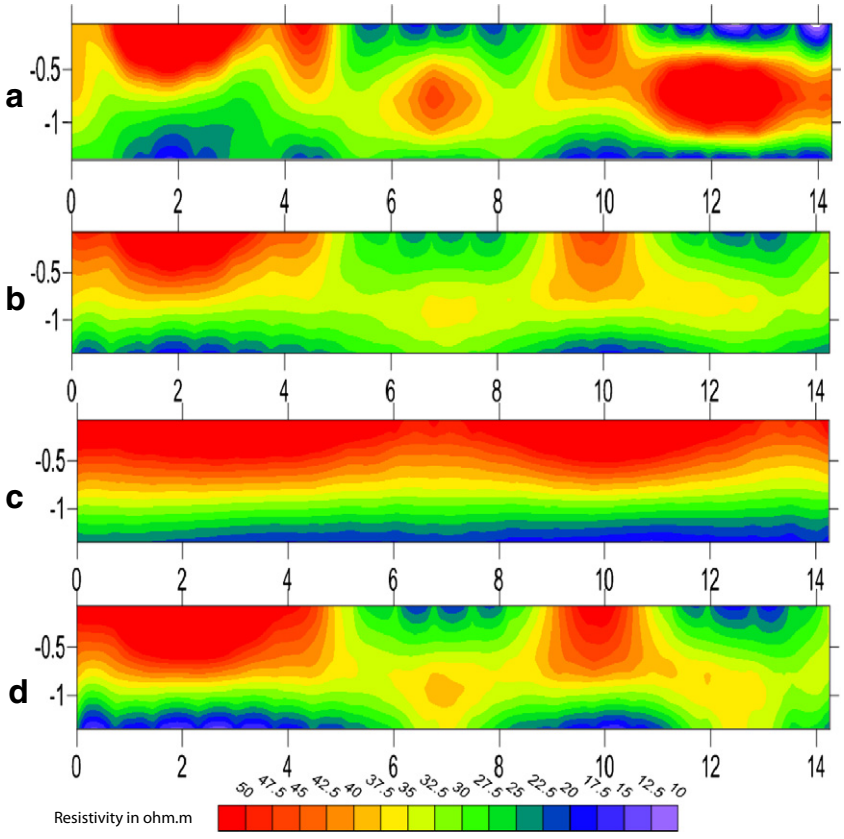

Fig. 9. 2-D resistivity models obtained by inverting the multi-height EM38 data shown in Fig. 8 using λ = a) 0.3, b) 3, and c) 30. d) Model obtained considering only data at heights corresponding to 0 and 0.3 m by using λ = 3. All models were obtained using 15 iterations.

water flow and the convection–dispersion equation for heat and solute transport. The Galerkin finite element method with linear basis functions is used to obtain a solution of the flow in Eq. (3) subject to the imposed initial and boundary conditions. Van Genuchten's Eqs. (4) and (5) were applied as retention and hydraulic conductivity functions in this model.

2.7. In-situ resistivity and degree of saturation relationship

To determine changes in soil moisture from ERT and EM38 images, we did not assume the validity of Archie's law. In fact, we established an in-situ approach based on resistivity and degree of saturation (S) changes by plotting the inverted value of resistivity of the extracted sample as a function of S. S is defined as:

$$S = \frac{\theta}{\varnothing} \tag{8}$$

where θ is the volumetric moisture content and ∅ is the porosity. The plot allowed us to obtain an empirical relationship between resistivity and S from the best match of the experimental data. To achieve this objective, we used the ERT and EM38 data collected right before sampling and then the inverted resistivity values of related pixels were extracted and plotted as a function of saturation to find out the best match of resistivity-S changes.

2.8. Geophysical and hydrological parameters

To evaluate which saturated hydraulic conductivity value represents field conditions, the moisture content distribution maps inferred from ERT and EM38 models were compared with simulating flow inferred from HYDRUS 2D using a misfit value:

$$\textit{Misfit error} = 100 * \sqrt{\sum_{i}^{N}\left[\left(\theta_s - \theta_g\right)^2\right]/N} \tag{9}$$

where θ_s is the simulated moisture content and θ_g is the moisture content inferred from ERT or EM38 models and N is the number of pixels of models. We compared the geophysical response and simulating flow in terms of which produces the smallest misfit. In addition, we calculated the percent of mass recovery of ERT and EM38 models in monitoring moisture content in order to provide a better quantitative comparison of geophysical models and simulating flow.

3. Results and discussion

3.1. Laboratory-measured soil properties

Soil samples at a distance of 6 and 9 m along from the start of the transect are shown in Figs. 4 and 5, respectively. The particle size distribution of all deep cores indicates a loam texture soil class composed of 25–50%, 35–55% and 15–25% concentration of sand, silt and clay respectively. The analysis of the third and fourth boreholes in 9 and 12 m shows a slightly greater sand concentration and lower amount of clay and silt contents than the first and second borehole in 3 and 6 m. The average concentration of sand, silt and clay in the first and second borehole is about 35%, 45% and 20% respectively while in the third and fourth borehole is 41%, 44% and 15% respectively. The average particle density and bulk density of samples were about 2.65 and 1.72 g/cm^3 respectively. Therefore, the average porosity was about 35%.

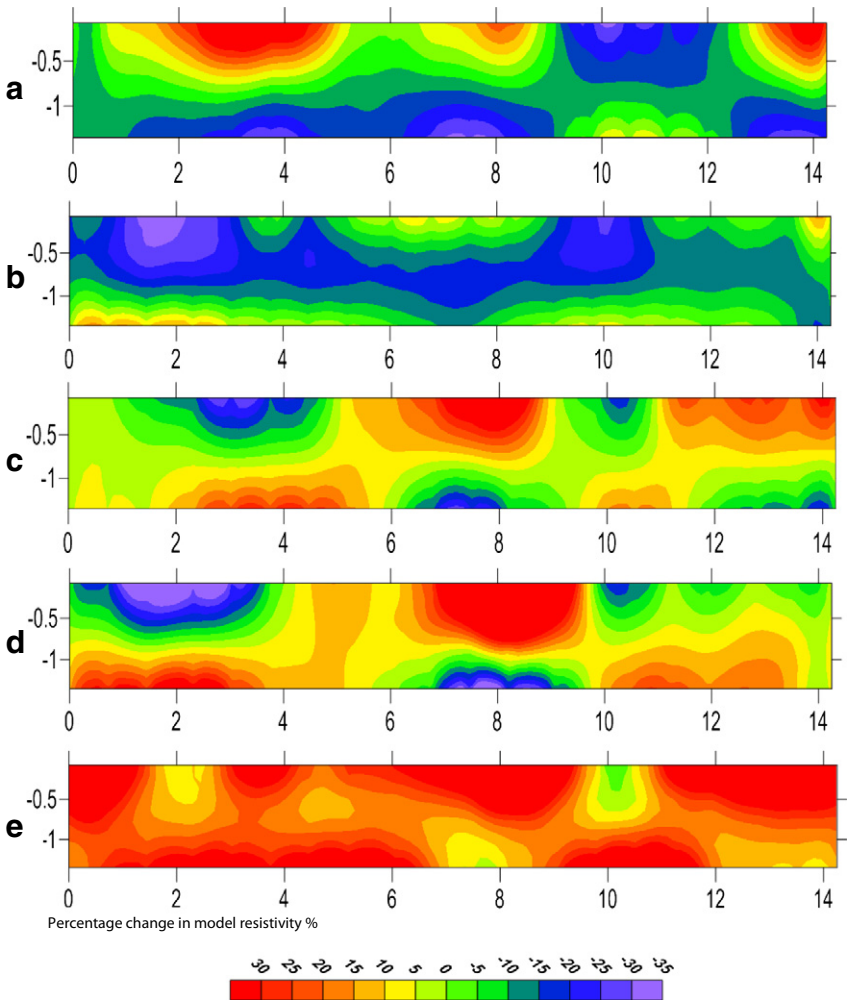

Fig. 10. Sequence of percentage resistivity changes inferred from inversion results using multi-height EM38 with respect to background in a) 4-Nov, b) 25-Nov 2010, c) 20-Jan d) 11-Feb and e) 20-Jun 2011.

3.2. Geophysical monitoring

The evolution of the moisture content distribution was monitored by the ground surface ERT and multi-height EM38 surveys since 28-Oct 2010 until 20-Jun 2011. If the equipment was available, ERT and EM38 were collected at the same day. Since the field site was a semi-pervious soil with a slow infiltration, the weekly measurement was carried out to trace the water movement. In some cases after the heavy rain, more datasets were collected to better monitor the water movement. A total of 45 and 40 surveys were carried out using ERT and EM38 methods during the experiment, respectively.

3.2.1. ERT

Fig. 6 shows the results of the background model achieved by inverting the ERT data collected using the 4POINTLIGHT_10W device on 28-Oct 2010. The modeling results show smooth resistivity variations along the profile. Greater resistivity values are seen on the right side of the models where the soil texture analysis also indicates lower clay content.

The time-lapse resistivity inversions in terms of percentage resistivity changes relative to the background ERT are presented in Fig. 7. This figure has four parts labeled a, b, c and d, which relate to data collected on 4-Nov 2010, 11-Feb, 21-Apr and 20-Jun 2011 respectively.

These data have been selected for the purpose of illustration, since data collected on these dates represent a more visible and different pattern of resistivity change in comparison with the background image. The first dataset (4-Nov 2010) was collected with a four day delay after three days of continuous rain amounting to 75, 60 and 10 mm. The second dataset (11-Feb, 2011) was collected after a two week delay and after rain. The third dataset was surveyed immediately after four days of continuous rain amounting to 25, 10, 7 and 31 mm. The last dataset was collected in the dry season.

Pattern observed in the first and third models in Fig. 7a and c reveals a decrease in resistivity in the middle zone and near the surface respectively due to the moisture content increase after rain. In contrast, there is no remarkable change in the second dataset in Fig. 7b. Finally the last models in Fig. 7d show a significant resistivity increase in the dry season. The resistivity increase on 20-Jun 2011 reveals a remarkable decrease of the moisture content in the dry season.

3.2.2. The EM38

The ECa (mS/m) data collected in 28-Oct 2010 using EM38 in vertical and horizontal modes of operation is shown in Fig. 8. Joint inversion of multi-height EM38 measurements was carried out using EM4Soil program. Data of each survey were inverted considering a same initial five-layer earth model. The first four layers were initialized with the same depth increment of 0.30 m and electrical conductivity of 15, 20, 25 and 35 mS/m respectively from the ground surface to depth. The electrical conductivity of the last layer was selected to be 50 mS/m. These values were estimated based on the ECa data collected by EM38 and also from the resistivity models in the previous section.

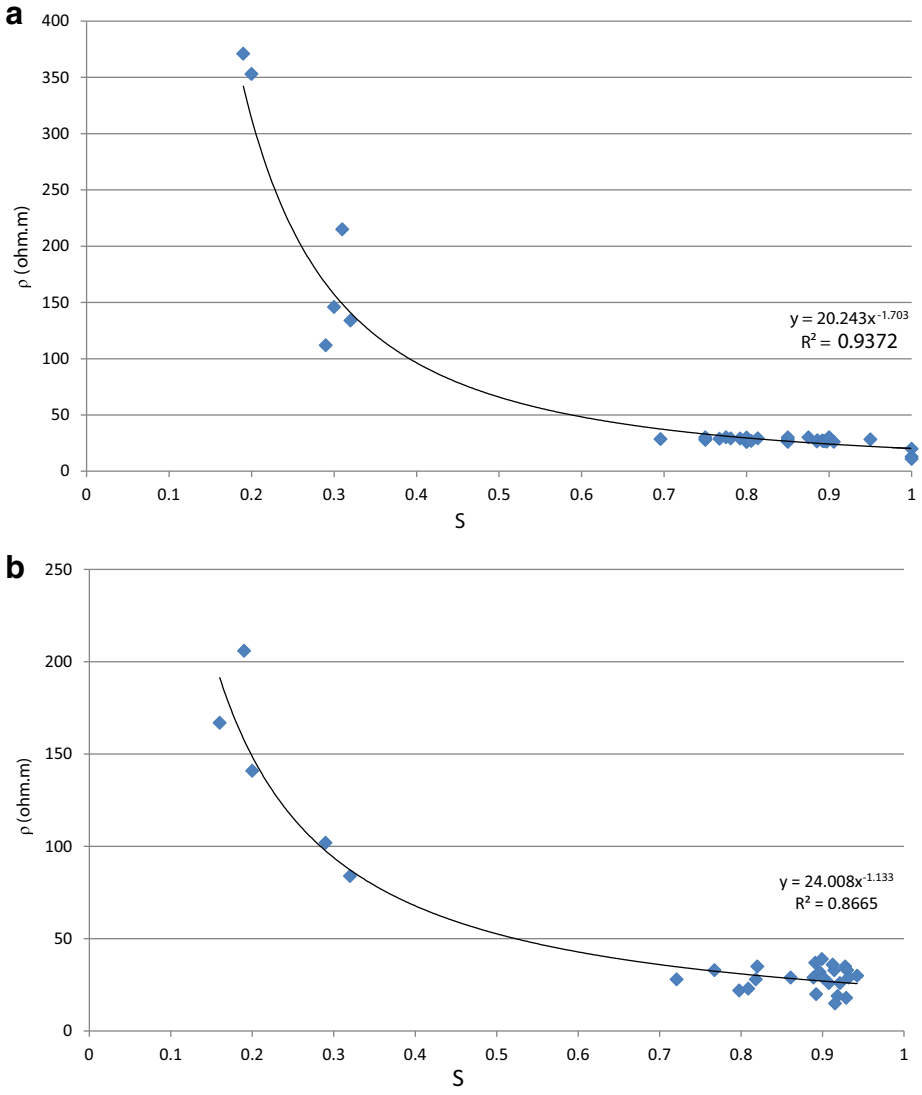

Fig. 11. Electrical resistivity of extracted samples as a function of the degree of saturation inferred from a) ERT models and b) EM38 models.

The inverted models of the first EM38 dataset measured in 28-Oct 2010 have been presented in Fig. 9. Fig. 9a, b and c was obtained using all 8 dataset and applying the 1-D laterally constrained inversion and using different values of damping factor (λ). Each model was obtained after 15 iterations. Fig. 9a was obtained using a small value of $\lambda = 0.3$ which corresponds to a less constrained inversion. The response of this model with total misfit of 4.85% shows a robust model with sharp changes along the profile. The background resistivity of this model is about 35 Ω.m and is reasonably consistent with the geoelectrical model shown in Fig. 6. Fig. 9b was obtained using $\lambda = 3$. The resistivity changes along the profile are smoother than the first model, but the lateral changes are still obvious in this model. The misfit error is slightly greater than the first model with 5.18%. Finally the last model using $\lambda = 30$ is shown in Fig. 9c. The high value of λ forces the calculation of a solution with a significant degree of smoothness for a more uniform model. The model shows very smooth changes along the profile and there is a substantial disagreement between model obtained using $\lambda = 30$ and geoelectrical model response in Section 3.2.1. The total misfit is 7.67% and is greater than the first and second models.

All EM38 datasets collected during the experiment, were inverted through the same procedure using $\lambda = 0.3$,3 and 30 (not shown here). We figured out that when $\lambda = 3$, the models well reflect the resistivity changes in our study. Although, small values of λ yield better fit, the lateral changes were exaggerated and artificial anomalies were produced in many cases. Furthermore, after finding the suitable value of λ, we inverted ECa datasets collected at height corresponding to the ground surface and 0.3 m. The time-lapse ECa data collected at height corresponding to 0.6 and 0.9 m indicated insignificant variations with less than 4 mS/m along the profile. In addition, the low values of ECa data at these heights are very sensitive to the setting and maintaining EM38 in Zero level noise. Therefore this insignificant spatiotemporal ECa variation for data collected at height corresponding to 0.6 and 0.9 m is not reliable where a quantitative model is required.

Fig. 9d shows the obtained model using ECa data collected at the ground surface and 0.3 m height with $\lambda = 3$. Our investigation reveals that using only these data reduces the total misfit error and slightly improves the models. Therefore, for further investigation we modeled ECa data collected in the vertical and horizontal modes of operation on the ground surface and 0.3 m height level by applying $\lambda = 3$. An investigation of EM38 background model in Fig. 9d shows smooth resistivity changes along the profile with the average of 30 Ω.m. The model shows a very good consistency with ERT models. Higher resistivity values are seen in the right and left upper zone of the profile.

Fig. 10 shows the results of multi-height EM38 data inversions in terms of percentage resistivity changes with regard to background.

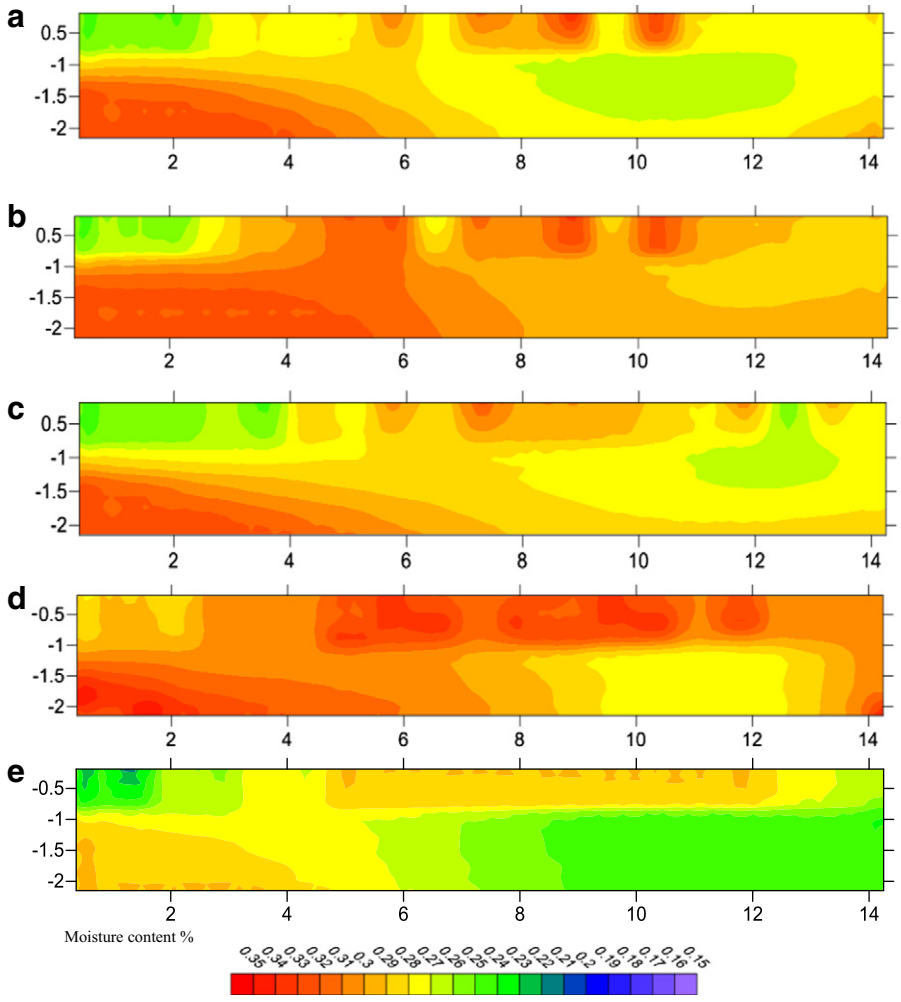

Fig. 12. 2-D moisture content distribution maps inferred from ERT models in a) 28-Oct and b) 4-Nov 2010, c) 11-Feb, d) 21-Apr and e) 20-Jun 2011 respectively.

This figure has five parts labeled a, b, c, d and e, which relate to data collected on 4 and 25-Nov 2010, 20-Jan, 11-Feb and 20-Jun 2011 respectively. The EM38 data in 4-Nov 2010, 11-Feb and 20-Jun 2011 were collected before ERT surveys in these days. Although there is some difference between resistivity variations inferred from EM38 and ERT models, pattern of results are reasonably similar. Both EM38 and ERT results show a decrease during the rain period in 4-Nov 2010 (Figs. 12b and 13b) and a significant increase in 20-Jun 2011 (Figs. 12e and 13f) in the dry season. The second dataset (25-Nov 2010) was collected after 12 days continuous rain amounting of 170 mm. The obtained model in this day shows the greatest resistivity decrease with regard to background during the experiment with an average of 20%. The maximum resistivity increase (about 20%) in both ERT and EM38 models is seen in the dry season on 20-Jun 2011 as expected.

3.3. In-situ resistivity and saturation relationship

In Fig. 11a, the inverted resistivity values of extracted sample were plotted as a function of S to find out the best match of resistivity-S changes. The obtained relationship is given by the following equation:

$$\rho_{ERT} = 20.243\, s^{-1.70} \tag{10a}$$

where S is the degree of saturation and ρ_{ERT} is the resistivity of the porous medium in relevant degree of saturation.

The same procedure was applied to determine changes in soil moisture from EM38 models. The resistivity-S changes were plotted in Fig. 11b. The obtained relationship for EM38 is given by the following equation:

$$\rho_{EM38} = 24\, s^{-1.133} \tag{10b}$$

Resistivity and S show weaker relationship in comparison with ERT models. Eqs. (10a), (10b) were used to convert resistivity changes to moisture content changes.

3.4. Moisture content distribution maps

The moisture content distribution maps were computed by converting ERT models using Eq. (10a). Fig. 12a, b, c, d and e shows the moisture content distribution maps for 28-Oct and 4-Nov 2010, 11-Feb, 21-Apr, and 20-Jun 2011 respectively. Maps of moisture content distribution clearly show how the moisture content of the unsaturated zone changes during the experiment. The moisture content decreased from an average of 28–32% in November to 22–27% in June. The right zone of the profile shows lower moisture content and greater variations during the experiment. Fig. 13a, b, c, d, e and f presents the moisture content distribution maps inferred from EM38 models using Eq. (10b) in 28-Oct, 4 and 25-Nov 2010, 20-Jan, 11-Feb and 20-Jun 2011 respectively. An investigation of calculated maps in Fig. 13 indicates that the

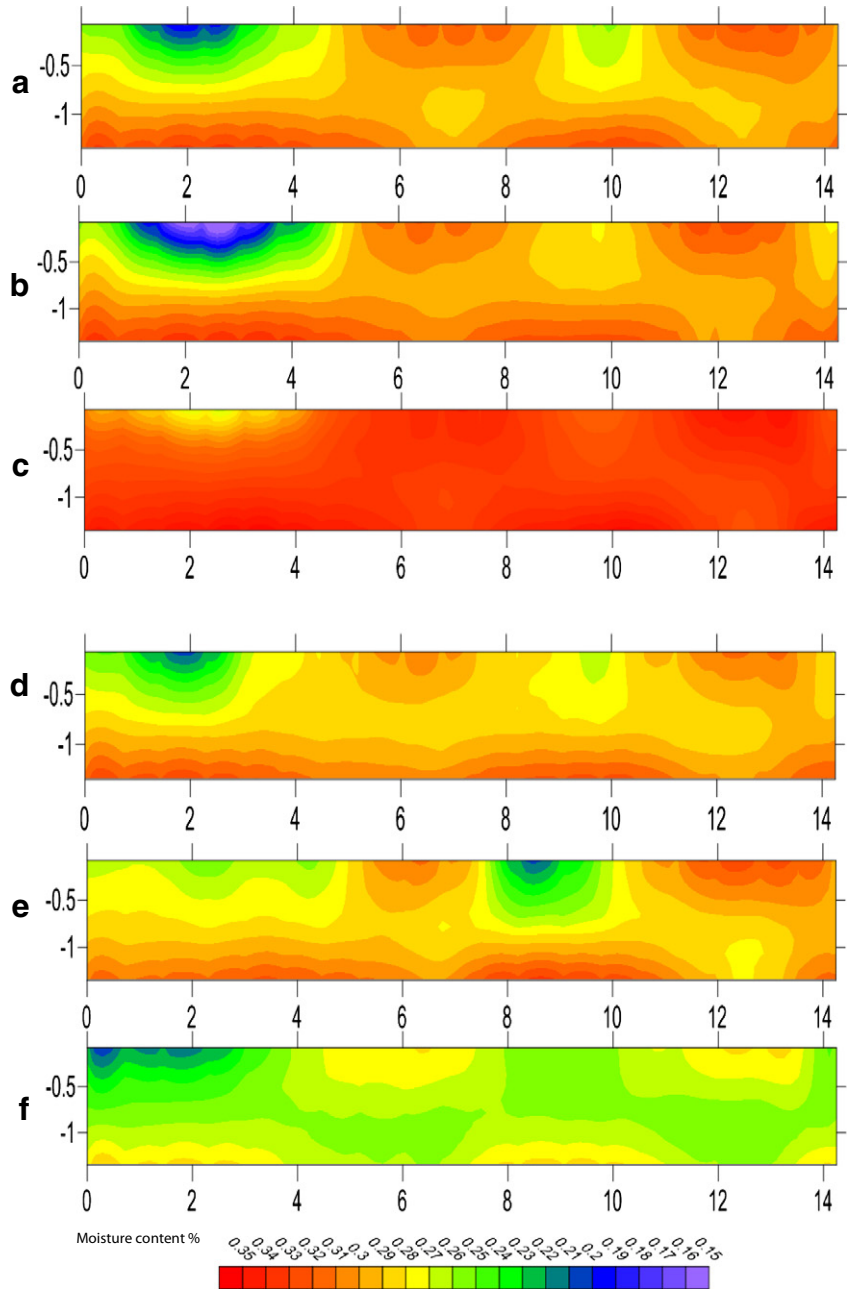

Fig. 13. 2-D moisture content distribution maps inferred from EM38 models in a) 28-Oct, b) 4-Nov and c) 25-Nov 2010, d) 20-Jan, e)11-Feb and f) 20-Jun 2011.

highest and lowest moisture content levels are seen in November and June respectively. The maps inferred from EM38 models displays less lateral resistivity changes along the profile in comparison with ERT models, yet the results are consistent. The spatiotemporal moisture content changes barely exceeded 10% during the experiment which indicates that the soil is semi-pervious and relatively homogeneous.

Table 1
Van Genuchten's parameters estimated by Rosetta.

Parameter estimation		θ_r	θ_s	α (cm^{-1})	n	k_s (cm/day)
a		0.041–0.05	0.33–0.36	0.01–0.02	1.32–1.45	3.5–8.25
b		0.046	0.35	0.015	1.35	4.5
c	0–7.5 m	0.048	0.35	0.015	1.36	4
	7.5–15 m	0.043	0.35	0.014	1.38	5.3

3.5. Estimating and constraining the hydrological parameters by geophysical data

To evaluate which saturated hydraulic conductivity value represent field conditions, unsaturated flow simulations were first built using HYDRUS 2D. Van Genuchten's parameters of each sample were first estimated using the Rosetta software. The ranges of van Genuchten's parameters of soil samples are presented in Table 1a. We simplified the soil texture to two scenarios. A homogeneous soil was considered first, assuming uniform hydraulic parameters throughout the investigated area (Table 1b). Close inspection of the grain size analyses from core sampling (as discussed in Section 3.1) and the geophysical models

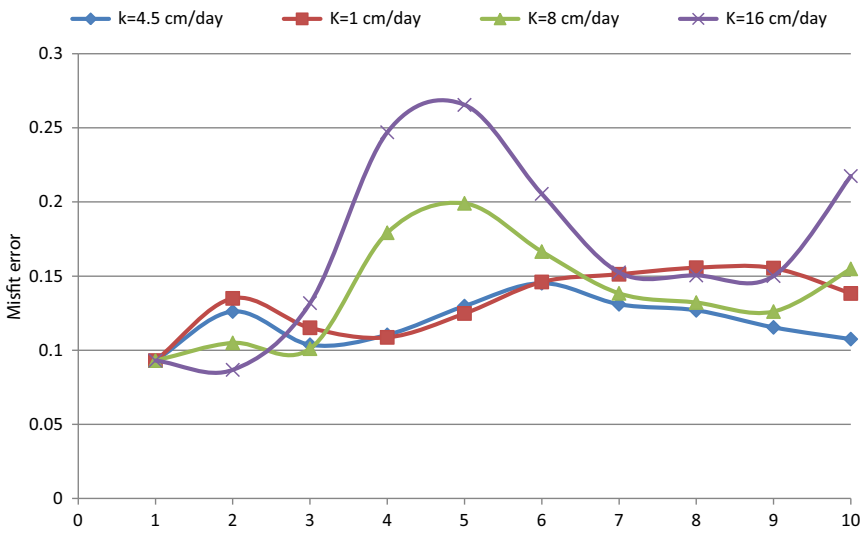

Fig. 14. Misfit error of moisture content distribution inferred from simulating flow and ERT models comparison. Four values of saturated hydraulic conductivity (K_s) and homogenous subsoil were used in these simulations.

indicated that the subsurface may be roughly subdivided into two soil zones with slightly different hydraulic characteristics.

We therefore divided the transect into two zones; the left side from 0–7.5 m and right side from 7.5–15 m. Estimated van Genuchten's parameters for each zone are given in Table 1c. Van Genuchten's equations along with estimated values were used as inputs of unsaturated flow simulation. Each simulation was initiated separately by using the moisture content distribution maps inferred from ERT and EM38 background images. Simulating the unsaturated flow, we used the same grid as the one used in ERT and EM38 inversions so as to make it possible to compare geophysical responses with flow simulations and evaluate the saturated hydraulic conductivity. The simulations were carried out for a 1.5 m of unsaturated soil, since the maximum investigation depth of EM38 was 1.5 m. The upper and bottom boundaries of the soil were simulated by implementing atmospheric and free drainage boundary conditions respectively.

All simulations were carried out for 238 days during 28-Oct 2010 to 20-Jun 2011 time period. Afterward, flow simulations were compared with the moisture content distribution maps inferred from ERT and EM38 models using Eq. (9).

Figs. 14 and 15 present a comparative illustration of the misfit error of simulating flow using the estimated van Genuchten's parameters for homogeneous soil (presented inTable 1b) and ERT and EM38 models. Among van Genuchten's parameters, the saturated hydraulic conductivity plays the most important role in dynamics of the unsaturated zone and in particular, it controls the speed of water infiltration. Therefore we fixed all of van Genuchten's parameters so as to make them the same as those shown in Table 1b. Afterwards, several new simulations were carried out by changing saturated hydraulic conductivity values to find the smallest misfit on the basis of the moisture content variations.

The percent of mass recovery of ERT and EM38 models in monitoring moisture content was also calculated and plotted in Figs. 16 and 17. An investigation of the misfit errors and present mass inferred from ERT models (Figs. 14 and 16) indicates that a saturated hydraulic conductivity value of 4.5 cm/day can reasonably reproduce the moisture content distribution during the experiment. Greater values of saturated

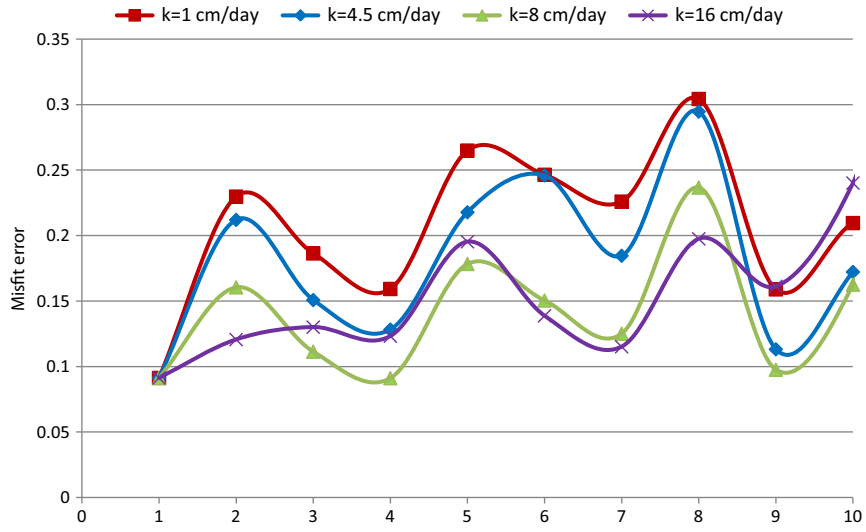

Fig. 15. Misfit error of moisture content distribution inferred from simulating flow and EM38 models comparison. Four values of saturated hydraulic conductivity (K_s) and homogenous subsoil were used in these simulations.

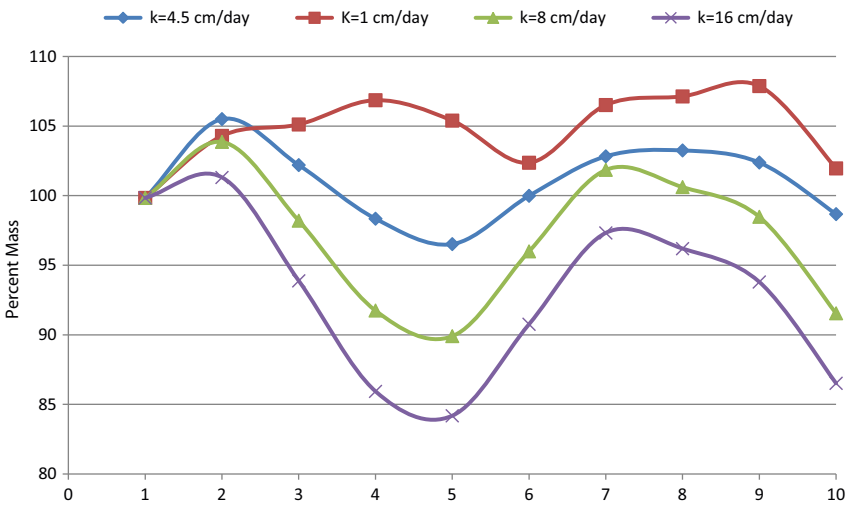

Fig. 16. Present mass recovery of moisture content distribution inferred from ERT models. Four values of saturated hydraulic conductivity (K_s) and homogeneous subsoil were used in these simulations.

hydraulic conductivity yield the higher misfit error and underestimate mass recovery while lower saturated hydraulic conductivity overestimates mass recovery of the moisture content distribution and increases the misfit error.

The results of EM38 models shown in Figs. 15 and 17 indicate that the saturated hydraulic conductivity of 8 cm/day can better reproduce the moisture content distribution during the experiment. Lower saturated hydraulic conductivity values overestimate mass recovery largely and show the greater misfit error. On the other hand, greater hydraulic conductivity underestimates mass recovery and also increases the misfit error. Saturated hydraulic conductivity estimated using EM38 models is greater than that estimated by ERT models, yet all results constrained hydraulic conductibility to be in 3–9 cm/day range.

We also calculated the misfit error and mass recovery of ERT models in comparison with simulating flow using 2-region soil and estimated van Genuchten's parameters in Table 1c. The misfit errors are shown in Fig. 18 with $\alpha = 1$.

Several new simulations were carried out using multiple values of saturated hydraulic conductivity shown in Table 1c. The goal was to find the smallest misfit and best mass recovery. Results indicate that the smallest misfit error and best mass recovery are achieved by a 2-region model with saturated hydraulic conductivity of 4 and 5.3 cm/day among our flow simulations. Comparing misfit error obtained using ERT models; we found that 2-region soil reproduced moisture content distribution slightly better than homogenous soil did.

We also investigated different scenarios for 2-region soil such as greater saturated hydraulic conductivity values for the left zone or greater differences between the saturated hydraulic conductivity values of the left and right zone (not shown here). Our investigation indicates that the saturated hydraulic conductivity of soil slightly increases among the profile from the left to the right side. We did the same procedure for EM38 models to analyze if they yield better fit with 2-region soil model. Different from ERT models, EM38 models did not better match to 2-region soil in our case study and the time-lapse EM38

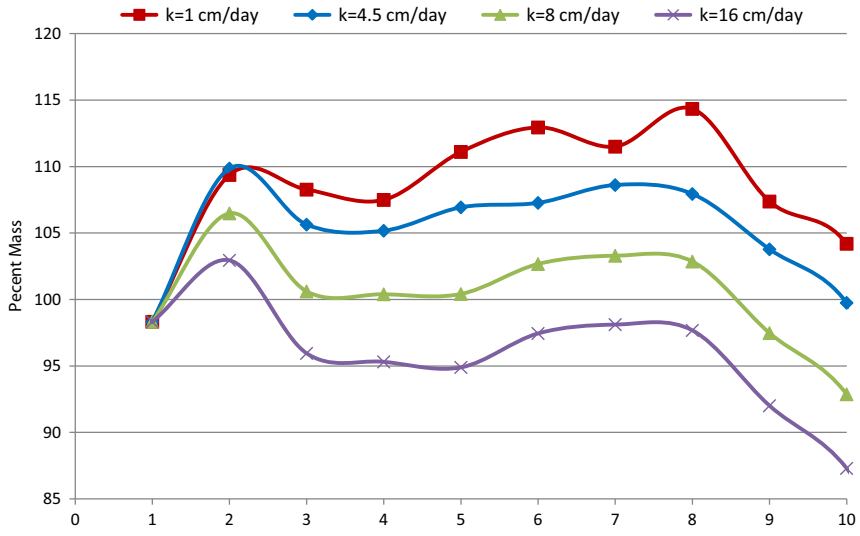

Fig. 17. Present mass recovery of moisture content distribution inferred from EM38 models. Four values of saturated hydraulic conductivity (K_s) and homogeneous subsoil were used in these simulations.

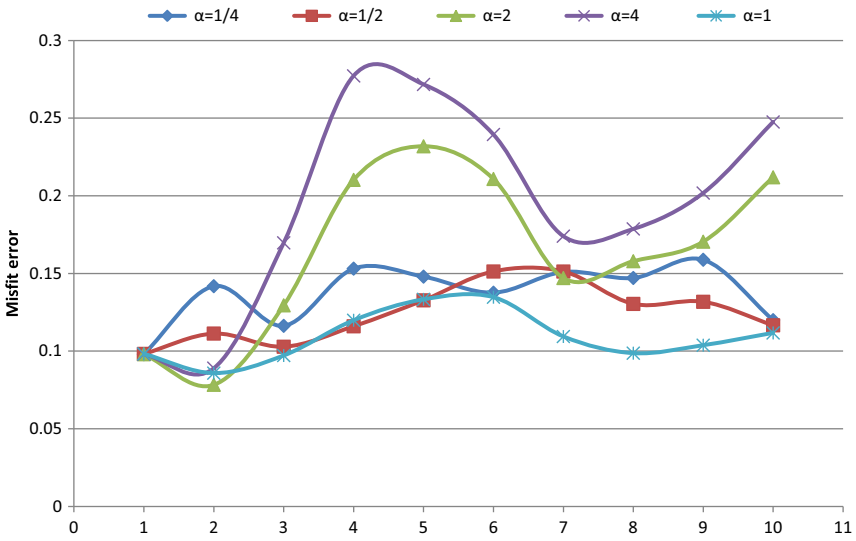

Fig. 18. Misfit error of moisture content distribution inferred from simulating flow and ERT models comparison. Five multiple values of hydraulic conductivity reported in Table 1c and 2-region subsoil were used in these simulations.

models did not present a pattern of lateral changes during the experiment. Lower inherent accuracy of EM38 in comparison with ERT surveys and the absences of time-lapse inversion algorithm for EM38 data contributed to creation of the discrepancy mentioned in these comparisons.

4. Conclusions

1. The experiment conducted at the campus of the University of Lisbon proves that the soil is semi-pervious sediment. The spatiotemporal moisture content changes during the experiment barely exceed 10%. Both EM38 and ground surface ERT methods were capable of imaging changes in bulk resistivity due to the moisture content variations. Our calculations using ERT and EM38 models constrain the range of the saturated hydraulic conductivity to be in 3–9 (cm/day); however the moisture content distribution maps inferred from ERT and EM38 models is to some extent different from flow simulations. This is not surprising because our simulations were limited to only homogenous and 2-region soil scenarios while a significant degree of heterogeneity had been observed in the soil texture analysis. In addition, the lateral water movement and the inversion process of ERT and EM38 data can explain this level of discrepancy. Moreover, the small contrast of the electrical conductivity between the excess moisture content and soil and also insufficient temporal variation under natural condition in this study added to the complication of using the ground surface ERT and EM38 methods in saturated hydraulic conductivity estimation.
2. Based on comparison of outcomes inferred from EM38 data and those from ERT method, EM38 proved to be acceptably capable in monitoring moisture content changes in shallow zone and estimating the hydraulic conductivity. Paying special attention to data collection and inversion algorithm is greatly important in order to achieve a quantitative model. Our investigation indicates that the obtained models using data collected in the vertical and horizontal modes of operation on the ground surface and 0.3 m height level and applying $\lambda = 3$ for data inversion well reflects the moisture content changes during the experiment. To the best our knowledge no attempt has been made to develop time-lapse inversions in EMI field. Developing a time-lapse inversion algorithm for EM38 data will be a concrete step for expansion of EM38 use in characterization of hydraulic variable properties where a multiple dataset is required.
3. We attempted to improve our approach by establishing an in-situ relationship for conversion of electrical conductivity to moisture content. This method has the advantage of using an approach same as ERT and EM38 models to calibrate field data which aims to reduce heterogeneity in moisture content distribution mapping. In contrast, the degree of saturation of extracted sample was limited and did not cover 0–1 range and also localizing the electrical conductivity of the related samples based on the inverted model was another source of uncertainty which made impractical to achieve a more accurate relationship. We also corrected the influence of temperature changes over ERT and EM38 models. The temperature data shows 20 °C variations during the experiment that affects significantly (about 40%) in ERT and EM38 models and was required to be modified for a quantitative mode.

Acknowledgments

The authors sincerely acknowledge the financial support from the grant of FCT (Referencia da bolsa: SFRH/BD/66665/2009) that made this study possible. We are grateful to Ivo Manuel Bernardo and Antonio Soares for continued support for our work. Thanks also to Vera Lopes from Geology Department, University of Lisbon who provided the laboratory facilities and useful guidance for samples analysis. The comments from anonymous reviewers are gratefully acknowledged.

References

Archie, G.E., 1942. The electrical resistivity log as an aid in determining some reservoir characteristics. J. Trans. Am. Inst. Miner. Eng. 146, 54–61.
Binley, A.M., Winship, P., Middleton, R., Pokar, M., West, J., 2001. High resolution characterization of vadose zone dynamics using cross-borehole radar. J. Water Resour. Res. 37 (11), 2639–2652.
Binley, A.M., Winship, P., West, L.J., Pokar, M., Middleton, R., 2002a. Seasonal variation of moisture content in unsaturated sandstone inferred from borehole radar and resistivity profiles. J. Hydrol. 267 (3–4), 160–172.
Binley, A.M., Cassiani, G., Middleton, R., Winship, P., 2002b. Vadose zone flow model parameterisation using cross-borehole radar and resistivity imaging. J. Hydrol. 267 (3–4), 147–159.

Binley, A.M., Kemna, A., 2005. DC resistivity and induced polarization methods. In: Rubin, Y., Hubbard, S.S. (Eds.), 50. Springer Hydrogeophysics Series: Water Science and Technology Library.
Brevik, E.C., Fenton, T.E., Lazari, A., 2006. Soil electrical conductivity as a function of soil water content and implications for soil mapping. J. Precis. Agric. 7, 393–404.
Cassiani, G., Strobbia, C., Giustiniani, M., Fusi, N., Crosta, G.B., Frattini, P., 2006. Monitoring of hydrological hillslope processes via time-lapse ground-penetrating radar. Boll. Geofis. Teor. Appl. 47 (1–2), 125–144.
Corwin, D.L., Lesch, S.M., 2005. Apparent soil electrical conductivity measurements in agriculture. J. Comput. Electron. Agric. 46, 11–43.
Deiana, R., Cassiani, G., Kemna, A., Villa, A., Bruno, V., Bagliani, A., 2007. An experiment of non invasive characterization of the vadose zone via water injection and cross-hole timelapse geophysical monitoring. J. NSGS 5 (3), 183–194.
Evett, S.R., Laurent, J., Cepuder, P., Hignett, C., 2002. Neutron scattering, capacitance, and TDR soil water content measurements compared on four continents. 17th World Congress of Soil Science, August 14-21, 2002, Bangkok, Thailand, pp. 1021-1–1021-10.
Fares, A., Alva, A.K., 2000. Soil water components based on capacitance probes in a sandy soil. Soil Sci. Soc. Am. J. 64, 311–318.
Fares, A., Buss, P., Dalton, M., El-Kadi, A.I., Parsons, L.R., 2004. Dual field calibration of capacitance and neutron soil water sensors in a shrinking-swelling clay soil. Vadose Zone J. 3, 1390–1399.
Hanson, B.R., Kaita, K., 1997. Response of electromagnetic conductivity meter to soil salinity and soil water content. J. Irrig. Drain. E ASCE. 123, 141–143.
Halvorson, A.D., Rhoades, J.D., 1974. Assessing soil salinity and identifying potential saline seep areas with field soil resistance measurements. J. Soil Sci. Soc. Am. 38, 576–581.
Hauck, C., 2002. Frozen ground monitoring using DC resistivity tomography. J. Geophys. Res. Lett. 29 (21), 2016.
Hayley, K., Bentley, L.R., Gharibi, M., Nightingale, M., 2007. Low temperature dependence of electrical resistivity: implications for near surface geophysical monitoring. J. Geophys. Res. Lett. 34 L18402.
Hayley, K., Bentley, L.R., Gharibi, M., 2009. Time-lapse electrical resistivity monitoring of salt-affected soil and groundwater. J. Water Resour. Res. 45, W07425.
Hayley, K., Pidlisecky, A., Bentley, L.R., 2011. Simultaneous time-lapse electrical resistivity inversion. J. Appl. Geophys. 75, 401–411.
Hezarjaribi, A., Sourell, H., 2007. Feasibility study of monitoring the total available water content using non-invasive electromagnetic induction-based and electrode based soil electrical conductivity measurements. J. Irrig. Drain. E ASCE 56, 53–65.
Huisman, J.A., Snepvangers, J.J.J.C., Bouten, W., Heuvelink, G.B.M., 2002. Mapping spatial variation of surface soil water content: comparison of ground-penetrating radar and time domain reflectometry. J. Hydrol. 269, 194–207.
Huisman, J.A., Sperl, C., Bouten, W., Verstraten, J.M., 2001. Soil water content measurements at different scales: accuracy of time domain reflectometry and ground-penetrating radar. J. Hydrol. 245 (1–4), 48–58.
Kemna, A., Vanderborght, J., Kulessa, B., Vereecken, H., 2002. Imaging and characterization of subsurface solute transport using electrical resistivity tomography (ERT) and equivalent transport models. J. Hydrol. 267 (3–4), 125–146.
Kim, J.H., Yi, M.J., Park, S.G., Kim, J.G., 2009. 4-D inversion of DC resistivity monitoring data acquired over a dynamically changing earth model. J. Appl. Geophys. 68, 522–532.
LaBrecque, D.J., Yang, X., 2001. Difference inversion of ERT data, a fast inversion method for 3-D in-situ monitoring. Eur. J. Environ. Eng. Geophys. 6, 83–89.
Loke, M.H., 1999. Time-lapse resistivity imaging inversion. Proceedings of the 5th Meeting of the Environmental and Engineering European Section, Em1.
Looms, M.C., Jensen, K.H., Binley, A.M., Nielsen, L., 2008a. Monitoring unsaturated flow and transport using cross-borehole geophysical methods. J. Vadose Zone 8, 227–237.
Looms, M.C., Binley, A.M., Jensen, K.H., Nielsen, L., Hansen, T.M., 2008b. Identifying unsaturated hydraulic parameters using an integrated data fusion approach on cross-borehole geophysical data. J. Vadose Zone 7, 238–248.
McNeill, J.D., 1980. Electromagnetic terrain conductivity measurement at low induction numbers. Technical Note TN-6.Geonics Limited, Mississauga, Ontario, Canada.
McNeill, J.D., 1986. Rapid, accurate mapping of soil salinity using electromagnetic ground conductivity meters. Tech. Note TN-18.Geonics Limited, Mississauga, ON, Canada.
Michot, D., Benderitter, Y., Dorigny, A., Nicollaud, B., 2003. Spatial and temporal monitoring of soil water content with an irrigated corn crop cover using surface electrical resistivity tomography. J. Water Resour. Res. 39 (5), 1138.
Monteiro Santos, F.A., 2004. 1-D laterally constrained inversion of EM34 profiling data. J. Appl. Geophys. 56, 123–134.
Mualem, Y., 1976. A new model for predicting the hydraulic conductivity of unsaturated porous media. J. Water Resour. Res. 12 (3), 513–522.
Muñoz-Carpena, R., 2004. Field devices for monitoring soil water content. Bulletin No. 343. Florida Cooperative Extension Service, Institute of Food and Agricultural Sciences, University of Florida.
Musgrave, H., Binley, A.M., 2011. Revealing the temporal dynamics of subsurface temperature in a wetland using time-lapse geophysics. J. Hydrol. 396, 258–266.
Oldenborger, G.A., Knoll, M.D., Routh, P.S., LaBrecque, D.J., 2007. Time-lapse ERT monitoring of an injection/withdrawal experiment in a shallow unconfined aquifer. J. Geophysics. 72, 177–188.
Reedy, R.C., Scanlon, B.R., 2003. Soil water content monitoring using electromagnetic induction. J. Geotech. Geoenviron. 129, 1028–1039.
Schaap, M.G., Leij, F.J., van Genuchten, M.Th., 2001. ROSETTA: a computer program for estimating soil hydraulic parameters with hierarchical pedotransfer functions. J. Hydrol. 251, 163–176.
Schön, J.H., 2004. Physical properties of rocks: fundamentals and principles of petrophysics. Seismic Exploration. vol. 18. Elsevier.
Sheets, K.R., Hendrickx, J.M.H., 1995. Non-invasive soil water content measurement using electromagnetic induction. J. Water Resour. Res. 31, 2401–2409.
Šimůnek, J., Šejna, M., van Genuchten, M.Th., 2006. The HYDRUS Software Package for Simulating Two- and Three-Dimensional Movement of Water, Heat, and Multiple Solutes in Variably-Saturated Media, User Manual, Version 1.0, PC Progress, Prague, Czech Republic.
Singha, K., Gorelick, S.M., 2006. Hydrogeophysical tracking of three-dimensional tracer migration: the concept and application of apparent petrophysical relations. J. Water Resour. Res. 42, W06422.
Triantafilis, J., Lesch, S.M., Lau, K.L., Buchanan, S.M., 2009. Field level digital soil mapping of cation exchange capacity using electromagnetic induction and a hierarchical spatial regression model. Aust. J. Soil Res. 47, 651–663.
Triantafilis, J., Monteiro Santos, F.A., 2010. Resolving the spatial distribution of the true electrical conductivity with depth using EM38 and EM31 signal data and a laterally constrained inversion model. J. Aust. Soil Res. 48, 434–446.
Triantafilis, J., Wong, V., Monteiro Santos, F.A., Page, D., Wege, R., 2012. Modelling the electrical conductivity of hydrogeological strata using joint inversion of loop–loop electromagnetic data. Geophysics 77, WB99–WB107.
Triantafilis, J., Terhune IV, C.H., Monteiro Santos, F.A., 2013. An inversion approach to generate electromagnetic conductivity images from signal data. Environ. Model. Softw. 43, 88–95.
Triantafilis, J., Monteiro Santos, F.A., 2013. Electromagnetic conductivity imaging (EMCI) of soil using a DUALEM-421 and inversion modelling software (EM4Soil). Geoderma 211–212, 28–38.
Van Genuchten, M.Th., 1980. A closed-form equation for predicting the hydraulic conductivity of unsaturated soils. J. Soil Sci. Soc. Am. 44, 892–898.
Wollenhaupt, N.C., Richardson, J.L., Foss, J.E., Doll, E.C., 1986. A rapid method for estimating weighted soil salinity from apparent soil electrical conductivity measured with an above ground electromagnetic induction meter. Can. J. Soil Sci. 66, 315–321.
Zhu, Q., Lin, H.S., Doolittle, J.A., 2010. Repeated electromagnetic induction surveys for improved soil mapping in an agricultural landscape. J. SWC 74 (5), 1763–1774.